Recent Winter Precipitation Changes over Eastern China in Different Warming Periods and the Associated East Asian Jets and Oceanic Conditions

DANQING HUANG

China Meteorological Administration–Nanjing University Joint Laboratory for Climate Prediction Studies, Institute for Climate and Global Change Research, School of Atmospheric Sciences, Nanjing University, Nanjing, China

AIGUO DAI

Department of Atmospheric and Environmental Sciences, University at Albany, State University of New York, Albany, New York, and National Center for Atmospheric Research, Boulder, Colorado

JIAN ZHU

State Key Laboratory of Hydrology–Water Resources and Hydraulic Engineering, Hohai University, Nanjing, China

YAOCUN ZHANG AND XUEYUAN KUANG

China Meteorological Administration–Nanjing University Joint Laboratory for Climate Prediction Studies, Institute for Climate and Global Change Research, School of Atmospheric Sciences, Nanjing University, Nanjing, China

(Manuscript received 13 July 2016, in final form 16 February 2017)

ABSTRACT

Global-mean surface temperature has experienced fast warming during 1985–98 but stabilized during 1999–2013, especially in boreal winter. Climate changes over East Asia between the two warming periods and the associated mechanisms have not been fully understood. Analyses of observation and reanalysis data show that winter precipitation has decreased (increased) over southern (northeastern) China from 1985–98 to 1999–2013. Winds at 300 hPa over East Asia strengthened during 1999–2013 around 30°–47.5°N but weakened to the north and south of it. This change pattern caused the East Asian polar front jet (EAPJ) and the East Asian subtropical jet (EASJ) to shift, respectively, equatorward and poleward during 1999–2013. Associated with these jet displacements, the Siberian high enhanced and the East Asian trough shifted westward. The enhanced Siberian high strengthened the East Asian winter monsoon and weakened southwesterly winds over the South China Sea, leading to precipitation decreases over southern China. The westward shift of the East Asian trough enhanced convergence and precipitation over northeastern China. A combination of a negative phase of the interdecadal Pacific oscillation and a positive phase of the Atlantic multidecadal oscillation during 1999–2013 resulted in significant tropospheric warming over the low and high latitudes and cooling over the midlatitudes of East Asia. These changes enhanced the meridional temperature gradient and thus westerlies over the region between the two jets but weakened them to the south and north of it, thereby contributing to the wind change patterns and the jet displacements.

1. Introduction

Eastern China is a densely populated region with a lot of agricultural and industrial activities. Variations in precipitation over eastern China often lead to severe droughts and floods, causing major damage in the region. Thus, it is important to investigate precipitation variability in eastern China and to understand its mechanisms. Since more rainfall occurs in summer than other seasons in eastern China, most studies have focused on summer precipitation by investigating its characteristics (e.g., Ding and Chan 2005; Ding et al. 2008) and controlling factors (e.g., Ding et al. 2009; Zhou et al. 2009; Ha et al. 2012), while relatively few studies have examined the variations in winter precipitation (Tao and Zhang 1998; Zeng et al. 2010; Ge et al. 2016; Ao and Sun 2016; C. Li et al. 2015). However, strong winter precipitation variability may also result in

Corresponding author: Dr. Danqing Huang, huangdq@nju.edu.cn

DOI: 10.1175/JCLI-D-16-0517.1

extreme events, such as the extreme snowstorm over southern China in January 2008 (Liao and Zhang 2013), the persistent drought over southern China from winter to spring in 2011 (Feng et al. 2014), and the frequent winter snowstorms over northeastern and northwestern China (Sun et al. 2010). These studies demonstrated the large impacts of anomalous winter precipitation during recent years.

Recently, many studies have highlighted the potential effect of global warming on winter precipitation variability (Wang and Fan 2013; Ding et al. 2014). X.-F. Li et al. (2015) found that the wetting trend over central eastern China during 1976–2009 can be largely attributed to the weakening of the East Asian winter monsoon (EAWM) in response to the warming in the tropical Indian Ocean. Liang et al. (2014) linked winter circulation variations (e.g., in East Asian trough, Siberian high, and East Asian jet) to different warming periods. Sun and Ao (2013) demonstrated that extreme winter precipitation has increased along with global warming in the past half century. It is well-known that global-mean surface temperature has experienced fast warming from the late 1970s to the 1990s (Hartmann et al. 2013), but the warming has slowed down since about year 2000, a phenomenon referred to as the ''global warming hiatus,'' which has attracted considerable attention during the last several years (Santer et al. 2011; Solomon et al. 2011; Gillett et al. 2012; Fyfe et al. 2012; Kosaka and Xie 2013; Trenberth and Fasullo 2013; England et al. 2014; Watanabe et al. 2014; Dai et al. 2015; Karl et al. 2015; Steinman et al. 2015). The hiatus phenomenon is most pronounced in boreal winter (Dai et al. 2015; X.-F. Li et al. 2015), and recent studies (e.g., Kosaka and Xie 2013; Dai et al. 2015; Steinman et al. 2015; Meehl et al. 2016) suggested that the transition from a warm to cold phase in the interdecadal Pacific oscillation (IPO) around 1999 and the recent phase change in the Atlantic multidecadal oscillation (AMO) played a major role for the recent slowdown in global warming rates. It is unclear how regional climate over eastern China responds to the two different warming rates before and after 1999, and the associated mechanism is also an open issue. Thus, from this perspective it is of interest to study recent winter precipitation changes over eastern China associated with the different warming periods before and after 1999.

Winter precipitation over China is influenced by various factors, one of which is the East Asian winter monsoon (Wang et al. 2010; Chen et al. 2013; Ding et al. 2014; C. Li et al. 2015). An anomalous EAWM can induce either cold or warm anomalies and affect winter precipitation over eastern China (Zhang et al. 1997; Huang et al. 2003; Zhou and Wu 2010; Zhou 2011). Generally, a weak EAWM is associated with anomalous southwesterly winds over the South China Sea, which enhance moisture convergence and increase precipitation over southern China (Tao and Zhang 1998; Zeng et al. 2010; Wang and He 2013). East Asian jets are key components of the EAWM (Kuang et al. 2008; Zhang et al. 2008). In winter, there are two jets located along the southern and northern side of the Tibetan Plateau (TP). They are the East Asian subtropical jet (EASJ) and the East Asian polar front jet (EAPJ) (Zou et al. 1990, 190–197; Hudson 2012). In general, a strong EASJ is accompanied by strong large-scale circulations, such as a strong Siberian high and East Asian trough, that can induce cold and dry anomalies over East Asia and lead to a strong EAWM (Chan and Li 2004; Mao et al. 2007; Kuang et al. 2008). Because of the wind divergence associated with the EASJ, its strengthening can stimulate upward movement at its exit region (Holton et al. 2002). Thus, the exact location of the EASJ is tightly coupled with that of the rain belt over East Asia (Yao and Li 2013). For the EAPJ, its intensity is highly correlated with winter precipitation over northeastern China (Zhang et al. 2008).

We noticed that both jets have experienced significant changes lately (Yu and Zhou 2007; Zhang and Huang 2011), such as the southward (Yu and Zhou 2007; Zhang and Huang 2011) and westward displacement (Du et al. 2009) of the EASJ around the late 1970s. Recently, R. Huang et al. (2014) reported that the EASJ has strengthened and the EAPJ has weakened since 1999, leading to a strengthened EAWM. However, it remains unclear whether there is any linkage between the changes of the EASJ and EAPJ and winter precipitation over China during the recent periods with differential warming. Recently, many studies have highlighted the importance of the concurrent variations of the EASJ and EAPJ (Liao and Zhang 2013; D.-Q. Huang et al. 2014; Li and Zhang 2014; Huang et al. 2015; Zhu et al. 2015; Wang and Zhang 2015). The concurrent variations reflect the interactions between the low- and high-latitude circulations over East Asia, and therefore they can lead to unique weather or climate patterns, including impacts on winter precipitation over eastern China (Liao and Zhang 2013; Luo and Zhang 2015).

Temperature variations can affect the meridional temperature gradient (MTG) (e.g., Seidel et al. 2008; Si et al. 2009; Yim et al. 2015) and therefore affect the variations of the EASJ and EAPJ through the thermal wind relation (Wallace and Hobbs 2005; Zhang and Huang 2011). In the lower troposphere, enhanced Arctic warming may contribute to the meridional displacements of the two jets (Yim et al. 2015) via the thermal wind relation (Overland and Wang 2010) and the baroclinic

changes (Woollings 2008; Woollings et al. 2014). Sea surface temperature (SST) variability in the Pacific and Atlantic Ocean can also affect the East Asian jets via the convective activities over the tropical oceans (Lu et al. 2013; D.-Q. Huang et al. 2014) and the baroclinic activities (Ren et al. 2010). Specifically, the IPO (Dai 2013) and AMO (Liu 2012) are the most pronounced modes for decadal–multidecadal SST variations, and they are generally considered as the major drivers of the recent decadal shifts of the EAWM (Sun et al. 2015). Previous studies have analyzed the impact of AMO and IPO on the EAWM, separately (Kim et al. 2014; Li and Bates 2007; Wang et al. 2008). They indicated that the EAWM strengthens (weakens) during the negative (positive) phases of the IPO or AMO (Ding et al. 2014). Thus, Arctic warming and IPO- and AMO-induced SST changes may alter meridional temperature gradients in the troposphere that affect the EASJ and EAPJ, which in turn could influence the EAWM and winter precipitation over eastern China. They can also directly alter winter land–ocean temperature gradients over East Asia, which affect the EAWM and thus winter precipitation over eastern China.

In this study, we aim to answer the following two questions: 1) How do the variations of the EAPJ and EASJ affect winter precipitation from the fast warming period to the hiatus period? 2) What are the possible mechanisms causing the variations of the EAPJ and EASJ? The rest of the paper is organized as follows. Section 2 describes the data and method. Winter precipitation and circulation anomalies during the different warming periods are presented in section 3. The linkage between the recent precipitation changes and the two jets is examined in section 4. In section 5, we propose a possible mechanism for the changes in the two jets. A summary and discussion are provided in section 6.

2. Data and method

a. Data

The datasets used in this study include the following products for the period from 1961 to 2013:

1) The second version of the gridded monthly precipitation dataset over China obtained from the China Meteorological Administration (http://data.cma.cn/site/index.html). This dataset is constructed based on quality-controlled rain gauge data from around 2400 stations over China and it is on a 0.5° grid (Zhao et al. 2014).
2) The global monthly Hadley Centre Sea Ice and SST dataset (HadISST) on a 1° × 1° grid derived from ship observations (Rayner et al. 2003).

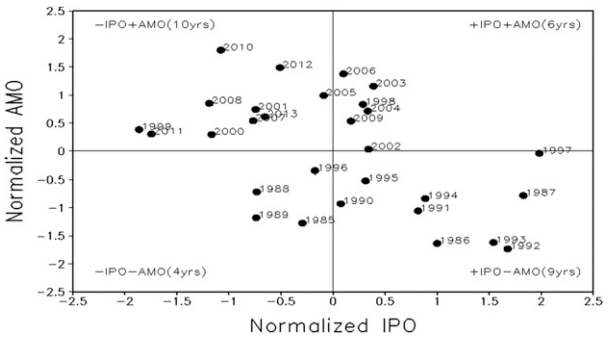

FIG. 1. The scatter diagram for the normalized winter IPO index against the normalized winter AMO index during 1985–2013.

3) The global monthly Hadley Centre/Climatic Research Unit surface temperature anomaly dataset, version 4 (HadCRUT4), on a 5° × 5° grid (Morice et al. 2012). It contains surface air temperature (from weather stations) over land and SST over ocean (from HadISST).
4) For comparison, two reanalysis datasets for upper-air daily and monthly fields are used in this study. They are the National Centers for Environmental Prediction (NCEP)–National Center for Atmospheric Research (NCAR) reanalysis on a 2.5° × 2.5° grid (Kalnay et al. 1996) and the ECMWF interim reanalysis (ERA-Interim) on a 1° × 1° grid (Dee et al. 2011). The analyzed variables include specific humidity, zonal and meridional wind components, vertical pressure velocity, air temperature, and sea level pressure (SLP).
5) The IPO and AMO index data are the same as those used in Dai (2013), Dai et al. (2015), and Dong and Dai (2015). They are smoothed principal components of the empirical orthogonal functions of the annual SST fields from 1920–2013 that represent the IPO and AMO patterns mainly in the Pacific and North Atlantic Ocean, respectively. To examine the combined effects of the IPO and AMO with different phases during 1985–2013, the 29 yr of data were divided into four different groups depending on the normalized IPO and AMO phase combination, as shown in Fig. 1. A composite analysis was carried out to examine the atmospheric circulation anomalies for each group.
6) The vertical tripole warming is defined as

$$\text{Vertical warming} = \overline{\Delta T}(0°\text{–}40°\text{N}) + \overline{\Delta T}(70°\text{–}80°\text{N}) - \overline{\Delta T}(45°\text{–}60°\text{N}), \quad (1)$$

where $\overline{\Delta T}$ (0°–40°N) is the mean winter temperature changes (1999–2013 minus 1985–98) averaged over

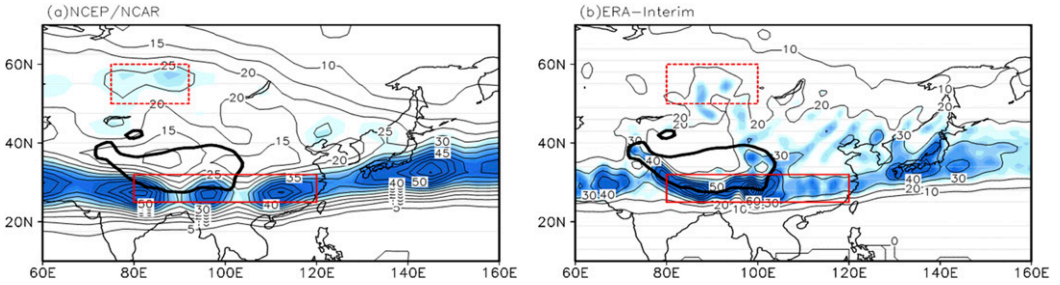

FIG. 2. Climatological number of boreal winter (DJF) jet cores at 300 hPa during 1985–2013 from (a) NCEP–NCAR reanalysis and (b) ERA-Interim datasets. Values above 24 are shaded in blue. The red solid (dashed) box indicates the active region of the EASJ (EAPJ). The thick black solid contour indicates the boundary of the Tibetan Plateau.

600–400 hPa for the East Asia (70°–140°E) sector between 0° and 40°N, and similarly for the other terms. To analyze the effect of vertical warming on 300-hPa winds, the normalized vertical warming is used.

b. Method

Following Ren et al. (2011), a jet core is identified if 1) the wind speed at 300 hPa is higher than 30 m s^{-1} for any given day and grid point and 2) the wind speed at the central point is larger than that at its eight surrounding points.

To select the key regions for the EAPJ and EASJ, the occurrence number of jet cores at each grid point in boreal winter [December–February (DJF)] is calculated using the daily data from the NCEP–NCAR reanalysis and ERA-Interim for 1985–2013 (Fig. 2). The reason for choosing the period 1985–2013 is explained in section 3. Figure 2 shows that the EASJ occurs more frequently than the EAPJ. The active region of the EAPJ is located over 50°–60°N, 75°–90°E (red dashed box in Fig. 2). There are two maximum jet core centers of the EASJ: one is located over the land along the southern flank of the TP (25°–32°N, 80°–120°E) and the other is located over the ocean along the Japanese archipelago (30°–37.5°N, 130°–160°E). A close relationship between the western branch of the EASJ and East Asian weather and climate has been revealed by many studies (D.-Q. Huang et al. 2014, 2015; Luo and Zhang 2015; Xiao and Zhang 2015). Thus, we focused on the western branch of the EASJ in this study. Specifically, the region of 25°–32°N, 80°–120°E (red solid box in Fig. 2) is chosen as the active region of the EASJ.

To quantify the meridional displacement of the EASJ and EAPJ, we used the latitude of the maximum wind speed at 300 hPa in the active region of the EAPJ and EASJ, respectively (referred to as the EAPJ/EASJ latitude axis), following Kuang and Zhang (2006). Before taking the latitude with maximum speed within the jet box, the wind speed field was spatially smoothed, which slightly reduces the year-to-year variations of the latitude axis.

The MTG over a tropospheric layer is estimated as $\Delta\overline{T}/R\Delta\phi$, where $\Delta\overline{T}$ is the difference of the vertically averaged temperature within the layer over a latitude band $\Delta\phi$, and R is Earth's radius. Regression analyses were performed over the 1985–2013 period to examine the relationship between the meridional displacements of the EAPJ or EASJ and the winter climate variations over eastern China. We also applied the following method to quantify the decadal contribution of the two jets to the decadal changes in winter precipitation over eastern China. For example, the regression function between the normalized EAPJ latitude axis X_{PJ} and precipitation Y_{PJ} is

$$Y_{\mathrm{PJ}} = \mathrm{A0}_{\mathrm{PJ}} + \mathrm{A1}_{\mathrm{PJ}} X_{\mathrm{PJ}}, \tag{2}$$

where $\mathrm{A0}_{\mathrm{PJ}}$ and $\mathrm{A1}_{\mathrm{PJ}}$ are the corresponding intercept and slope of the regression, respectively. We used Eq. (2) to estimate the mean precipitation anomaly ΔY_{PJ} associated with a jet change:

$$\Delta Y_{\mathrm{PJ}} = \mathrm{A1}_{\mathrm{PJ}} \Delta X_{\mathrm{PJ}}, \tag{3}$$

where ΔX_{PJ} is the decadal shift (1999–2013 minus 1985–98) of the EAPJ axis latitude. Thus, ΔY_{PJ} represents the contribution of the EAPJ shift to the decadal precipitation change. Similarly, the contribution of the EASJ shift ΔY_{SJ} can also be estimated. Then ΔY_{SJ} and ΔY_{PJ} are combined to represent the concurrent contribution of the EAPJ and EASJ shifts. Since the time series of the EAPJ and EASJ latitude axes are only weakly correlated (see Fig. 8), it is reasonable to simply combine their contributions estimated through Eq. (3) to derive the total contribution due to their meridional displacements. The combined contribution is similar to that estimated using a multiple regression between the precipitation anomaly and the positions of the two jets. The same method was also used to quantify the contributions of the decadal changes in the IPO and AMO (as X) to the decadal displacements of the two jets (as Y).

An EOF analysis was applied to extract the dominant modes of winter precipitation over eastern China in

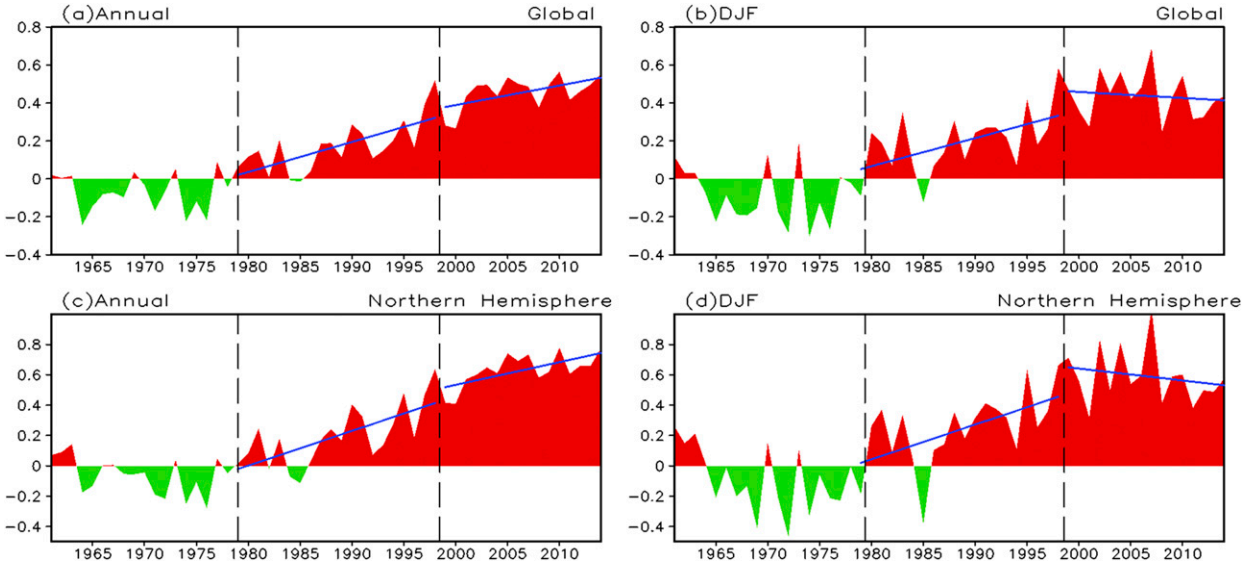

FIG. 3. The (a),(b) global mean and (c),(d) the Northern Hemisphere mean of (a),(c) annual and (b),(d) boreal winter (DJF) surface temperature anomalies (°C; relative to 1961–90 mean) from HadCRUT4 during 1961–2013. The two vertical dashed lines in (a)–(d) indicate the years of 1979 and 1998. The blue solid lines in (a)–(d) indicate the trends in the two warming periods.

1985–2013. The Mann–Kendal test (Mann 1945; Kendall 1975) was applied to detect the abrupt changepoint of the decadal variation.

3. Recent winter precipitation and circulation changes

To analyze the precipitation changes between the fast warming and hiatus periods, we first defined the two periods. Figures 3a and 3b show the global-mean surface temperature anomalies during 1961–2013 for annual and winter mean, respectively. During 1961–2013, separated by dashed vertical lines in Fig. 3, there are three periods with distinct warming rates: a cold period from 1961 to 1977 with little change, a fast warming period from 1978 to 1998, and a hiatus period from 1999 to 2013. The third period is with little warming for annual and slightly cooling for winter. That is why we focus on the circulation changes in DJF. The three warming periods are in accordance with previous studies (e.g., Li et al. 2007; Ma et al. 2012; Zhang 2016). Similar warming patterns are also seen over the Northern Hemisphere (Figs. 3c,d). The volcanic eruptions in 1963, 1982, and 1991 caused temporal cooling for a few years after each event. To eliminate the temporal cooling after 1982, we chose two nearly 15-yr periods: namely, 1985–98 as the fast warming period and 1999–2013 as the hiatus period. This division is also consistent with the results of Ding et al. (2014) and C. Li et al. (2015). In the following, all the decadal changes are the 1999–2013 mean minus the 1985–98 mean.

Climatological mean winter precipitation over eastern China decreases gradually from the south to the north, with a high precipitation center over southeastern China (Fig. 4a). In Fig. 4b, differences of winter precipitation between the two warming periods show widespread decreases over southern China, the midwest reaches of the Yangtze River, and the southeast corner of northern China. Over southern China, the winter precipitation has decreased by approximately 25%. This is consistent with the frequent drought events in recent years over southern China, as noticed previously (e.g., Xin et al. 2006; Feng et al. 2014; Huang et al. 2015). However, winter precipitation has increased by approximately 50% over northeastern China during the hiatus period (Fig. 4b). Specifically, another wet anomaly center is also indicated in the Yangtze River delta. This coincides with the wetting trend in the period of 1976–2009 reported by X.-F. Li et al. (2015), who revealed that the increasing SST in the Indian Ocean was largely responsible for the recent precipitation increase over the Yangtze River delta. The warming of the Indian Ocean causes an anomalous cyclonic circulation along the coast of eastern China and brings more water vapor there. In this study, besides the Yangtze River delta, we mainly focused on the much wider regions, which are northeastern China (40°–54°N, 120°–135°E) with wet anomalies and southern China (20°–28°N, 105°–122°E) with dry anomalies during the hiatus period. The top parts of Figs. 4c and 4d show the time series of regional-mean winter precipitation averaged over northeastern China and southern China, respectively. They show that the

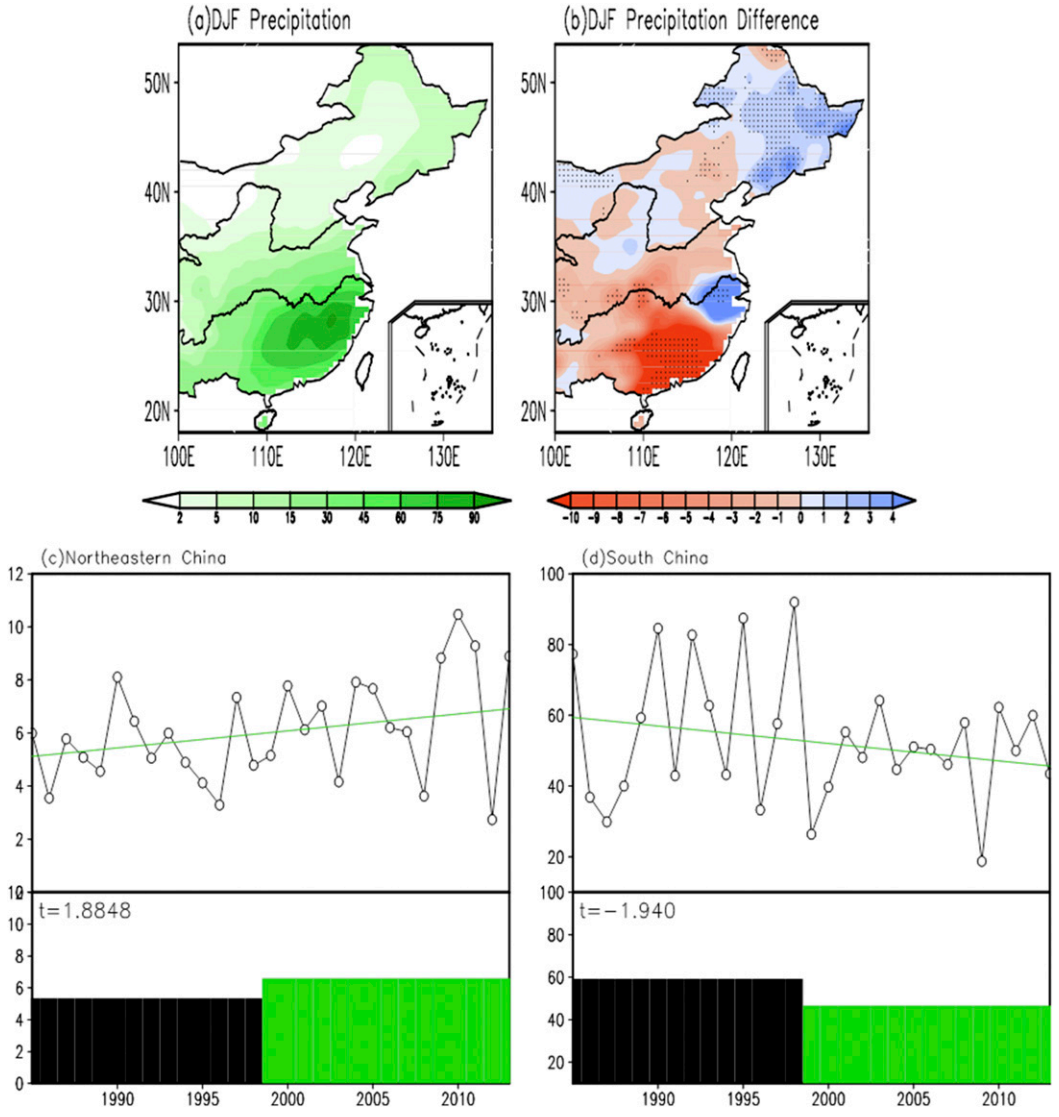

FIG. 4. The 1985–2013 mean winter (DJF) precipitation over (a) eastern China (mm), (b) precipitation difference (mm) between 1999–2013 and 1985–98, and the time series of the regional-mean winter precipitation averaged over (c) northeastern China (40°–54°N, 120°–135°E) and (d) southern China (20°–28°N, 105°–122°E) for 1985–2013. The dots in (b) indicate that the difference is significant at the 90% level. The green lines in (c),(d) are linear trends. The black (green) bars in (c),(d) indicate the mean winter precipitation in 1985–98 (1999–2013).

linear trend of winter precipitation is positive over northeastern China but negative over southern China. However, both trends are insignificant statistically. The Student's t test values of the precipitation changes between the two periods (bottom parts of Figs. 4c,d) indicate that the regime shift in the two regions is significant, and the shift results mainly from decadal variations with small contributions from long-term trends. An analysis of the regional precipitation data from 1961 to 2013 confirmed this conclusion (results not shown).

We further performed an EOF analysis to quantify the dominant modes of winter precipitation variations over eastern China during 1985–2013. As shown in Fig. 5a, the leading mode (EOF1) accounts for 51% of the total variance and is well separated from the other modes by the criterion defined by North et al. (1982). It shows a southern-dry–northeastern-wet precipitation anomaly pattern. The first principal component (PC1) associated with EOF1 exhibits both interannual and interdecadal variations (Fig. 5b). Though the regime shift around 1999 in PC1 is not significant based on the Mann–Kendall test (Fig. 5c), the PC1 is mostly with negative (positive) anomalies before (since) 1999. The second EOF (EOF2; Fig. 5d) shows a dipole pattern with two large centers:

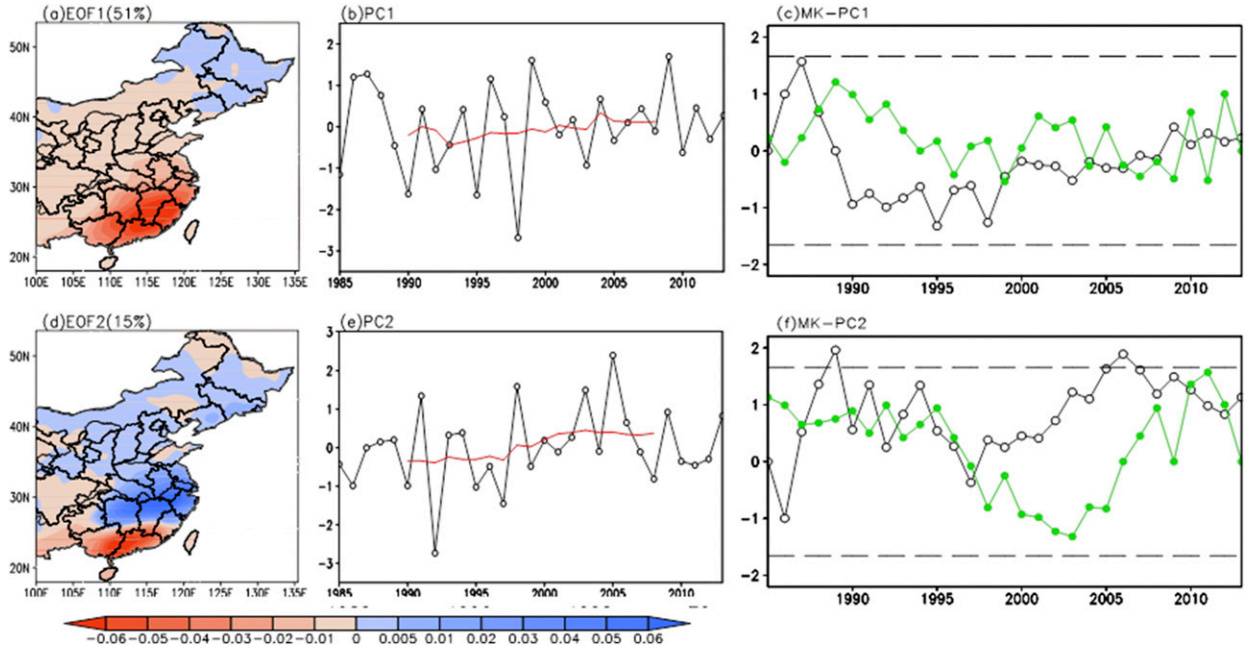

FIG. 5. The spatial patterns of the (a) first and (d) second leading EOF modes of winter precipitation during 1985–2013; (b),(e) the corresponding time series of the PCs; and the Mann–Kendall test (MK) of (c) PC1 and (f) PC2. The red lines in (b),(d) indicate the 11-point running average. The two black dashed lines in (c),(f) indicate the 90% confidence level of the MK.

southeastern China and the Yangtze River delta. This mode also shows a decadal shift around 1999 (Fig. 5e). The regime shift around 1999 in PC2 is statistically confirmed by the Mann–Kendall test (Fig. 5f). Thus, the EOF analysis also confirms that there exists a regime shift around 1999 in winter precipitation over eastern China, and the decadal difference results mainly from multidecadal variations, not from a secular long-term trend.

The large-scale circulation changes between the two periods (Fig. 6) favor the northeastern-wet–southern-dry anomaly pattern, as one would expect. As shown in Figs. 6a,b, negative geopotential height anomalies of about 20 gpm at 500 hPa are located over regions around 40°–60°N, 100°–140°E, covering parts of northeastern China. These height anomalies move the East Asian trough (red line in Figs. 6a,b) westward and slightly tilt toward northeastern China. This could help trigger more ascending movement, which can be seen in vertical wind fields (not shown), and thus enhance precipitation over northeastern China during the hiatus period. In contrast, positive height anomalies are seen over southern China (Figs. 6a,b), which could suppress upward motion and reduce precipitation there. Meanwhile, positive height anomalies cover high-latitude Eurasia and the subtropical regions in the sector (Figs. 6a,b). These height anomalies are associated with an increase (decrease) in the meridional height gradient from low to middle (middle to high) latitudes; thus they should strengthen the EASJ but weaken the EAPJ.

Near the surface (Figs. 6c,d), large positive SLP anomalies (up to 4 hPa) dominate high-latitude Eurasia, including the Siberian regions, while negative anomalies of approximately 2 hPa cover the low latitudes. This strengthens the Siberian high (located over 40°–50°N, 80°–110°E) and expands it poleward during the hiatus period. The increased height over high-latitude Eurasia at 500 hPa also implies a strengthened Siberian high at the surface. As the Siberian high strengthens, the EAWM should strengthen with increased northeasterly winds over most of eastern China (Luo and Zhang 2015). Consequently, southwesterly winds should weaken over the South China Sea, and precipitation should decrease over southern China (Tao and Zhang 1998; Zeng et al. 2010; Wang and He 2013). Our analyses based on some EAWM indices (Wang and Chen 2010; Shao and Li 2012) also revealed significant strengthening of the EAWM during the hiatus period (not shown). The results are consistent with Ding et al. (2014), who showed that the EAWM had experienced decadal changes, with weakening after the mid-1980s and strengthening after about 2005.

4. Link between recent precipitation changes and the EAPJ and EASJ

To explore whether the precipitation and circulation changes are related to the variations of the EASJ

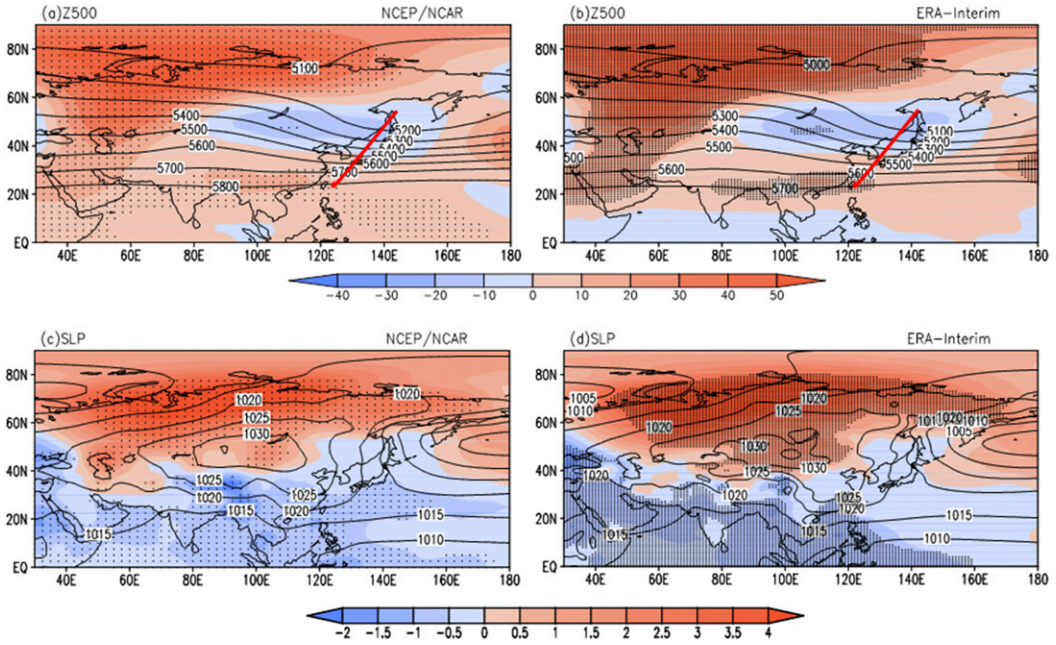

FIG. 6. (a),(b) The 1985–2013 mean DJF geopotential height at 500 hPa (contours, gpm) and its change (shading, gpm; 1999–2013 minus 1985–98), (c),(d) the 1985–2013 mean DJF sea level pressure (contours, hPa) and its change (shading, hPa; 1999–2013 minus 1985–98) from (left) NCEP–NCAR reanalysis and (right) ERA-Interim datasets. The dots indicate that the difference is significant at the 90% level. The red line in (a),(b) indicates the approximate mean location of the East Asian trough in the DJF 500-hPa height field.

and EAPJ, we first examined wind speed changes at 300 hPa between the two periods. Figure 7 shows a tripole alternating zonal pattern with strengthened winds around 30°–47.5°N (midlatitude) and weakened winds to the north and south of it. This negative–positive–negative wind anomaly pattern from 10° to 60°N causes meridional displacements of the two jets, with an equatorward shift of the EAPJ and a poleward shift of the EASJ during the hiatus period. We noticed that the geopotential high changes at 300 hPa (not shown) were similar to those at 500 hPa (Figs. 6a,b). The low pressure anomaly center over 40°–60°N, 100°–140°E should induce a cyclonic wind anomaly over the area between the two jets. This cyclonic wind anomaly should lead to wind speed changes, as shown in Fig. 7.

Figure 8 shows the time series of the latitude axis of the EASJ and EAPJ during 1985–2013. Besides an equatorward (poleward) shift of the EAPJ (EASJ) from 1985–98 to 1999–2013, which is more evident in the ERA-Interim data than in the NCEP–NCAR reanalysis, Figs. 8a,b also show that the interannual variations of the latitudinal position of the EAPJ has increased during the hiatus period. This increased variability is consistent with the large interannual variations in the cold breaks and winter precipitation over China in recent years (Wang and Feng 2011). Compared with the large interannual variations, the decadal shifts shown in Fig. 8 are statistically insignificant, except Fig. 8d, which is significant at the 90% level. However, this does not mean that these shifts cannot have a significant impact on winter climate over eastern China.

To examine the relationship between the meridional displacement of the EAPJ and EASJ and winter precipitation changes over eastern China, we regressed winter precipitation against the normalized latitude axis of the two jets separately. Figure 9a shows that, associated with an equatorward displacement of the EAPJ, winter precipitation increases over northeastern China. In contrast, associated with a poleward displacement of the EASJ, winter precipitation decreases over southern China (Fig. 9b). The regression patterns are similar with the ERA-Interim data (not shown).

Associated with the equatorward displacement of the EAPJ, 500-hPa geopotential height decreases over mid-to-high-latitude Asia around 47.5°–60°N, especially to the west of Lake Baikal, but increases over the polar region around 60°–80°N, 90°–140°E (Fig. 9c; same for ERA-Interim). Associated with the poleward displacement of the EASJ, 500-hPa height also decreases over a region around Lake Baikal (Fig. 9d; or to the east of Lake Baikal for ERA-Interim, not shown). Meanwhile, 500-hPa height increases over the high

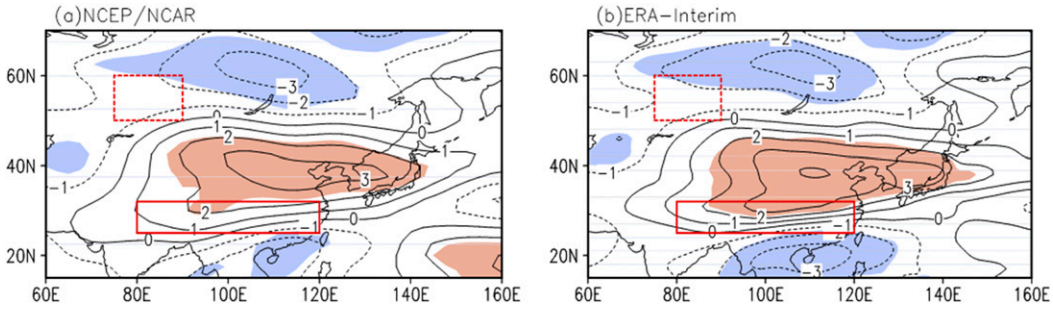

FIG. 7. The DJF wind speed difference (m s^{-1}) at 300 hPa between 1999–2013 and 1985–98 from the (a) NCEP–NCAR reanalysis and (b) ERA-Interim. The red solid (dashed) box indicates the active regions of the EASJ (EAPJ). The shading indicates that the difference is significant at the 90% level.

latitudes (60°–80°N, 30°–110°E) and the mid-to-low latitudes (20°–40°N) (Fig. 9d). The negative height anomalies around Lake Baikal associated with the displacements of both the EAPJ and EASJ may shift the East Asian trough (cf. Figs. 6a and 6b) westward and strengthen it.

Near the surface, positive SLP anomalies over high-latitude Eurasia are associated with both the equatorward displacement of the EAPJ and the poleward displacement of the EASJ (Figs. 9e,f), particularly for the ERA-Interim dataset (not shown). This suggests a strengthening and poleward expansion of the Siberian high (cf. Figs. 6c and 6d), which is also reflected by increased height at 500 hPa over the polar region (Figs. 9c,d). These results are consistent with the findings of Luo and Zhang (2015), who showed that an equatorward shift of the EAPJ concurred with an enhanced Siberian high at the surface, which in turn strengthened the EAWM. A strengthened EAWM with enhanced northeasterly winds would weaken southwesterly winds over the South China Sea and decrease precipitation over southern China (Tao and Zhang 1998; Zeng et al. 2010; Wang and He 2013).

To quantify the contributions of the meridional displacements of the two jets to the decadal changes in precipitation (Fig. 4b) and the circulations (Fig. 6), we multiplied the regression coefficients shown in Fig. 9 by the decadal changes in the position of the two jets from 1985–98 to 1999–2013 (Fig. 8) and combined

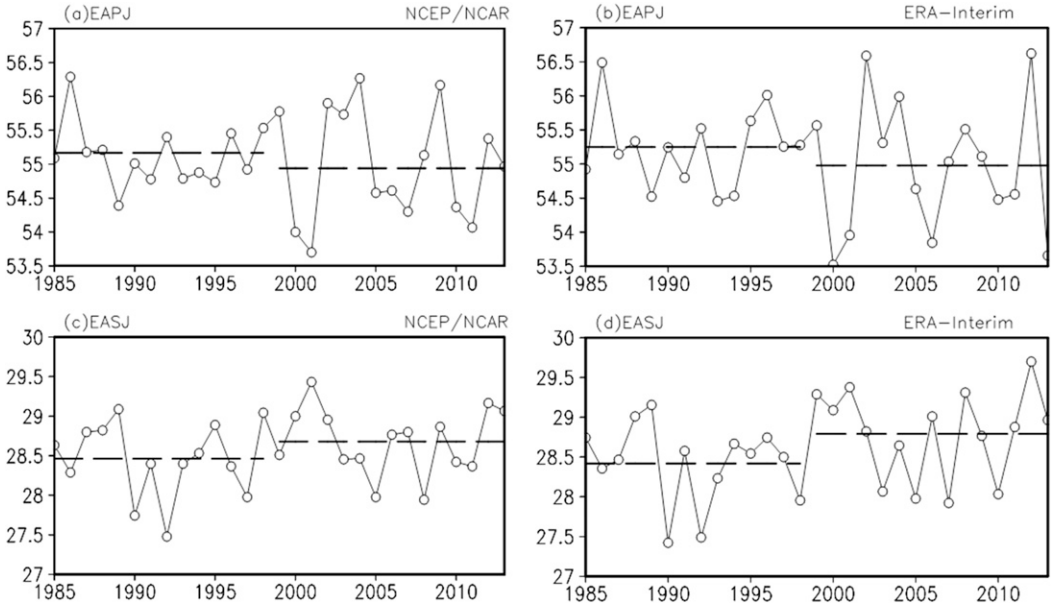

FIG. 8. The latitude (°N) of the DJF (a),(b) EAPJ and (c),(d) EASJ during 1985–2013 from the (left) NCEP–NCAR reanalysis and (right) ERA-Interim datasets. The two dashed lines indicate the mean value of the latitude axis of the EAPJ and EASJ for 1985–98 and 1999–2013. The correlation coefficient between the EAPJ and EASJ series is −0.16 and −0.06 for the NCEP–NCAR and ERA-Interim cases, respectively.

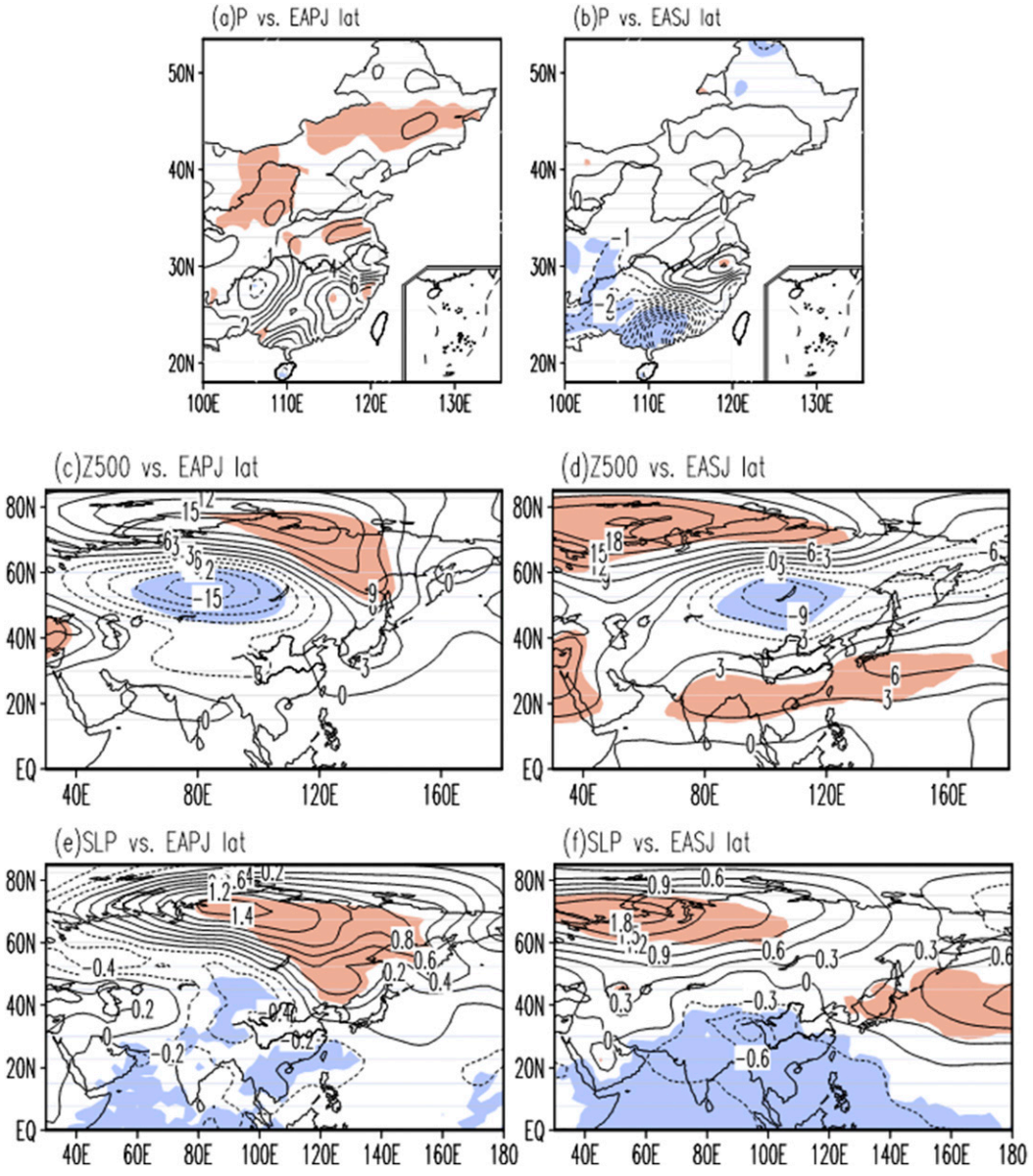

FIG. 9. Regression coefficients of (a),(b) DJF precipitation (mm day^{-1}); (c),(d) geopotential height at 500 hPa (gpm); and (e),(d) SLP (hPa) against the normalized latitude axis of the (left) EAPJ (multiplied by −1, indicating the poleward displacement of EAPJ) and (right) EASJ for 1985–2013 from the NCEP–NCAR reanalysis dataset. The shading indicates that the regression coefficient is significant at the 90% level.

them to show the effect of the decadal shifts of the two jets in Fig. 10. This method is acceptable because the two time series of the jet axis (Fig. 8) are only weakly correlated. A multiple regression of the precipitation or circulation fields against the two jet locations yielded similar results (not shown) for the combined contribution, further confirming the reliability of the above method. The estimated changes of precipitation (Figs. 10a,b) and circulation (Figs. 10c–f) associated with the jet shifts are broadly consistent with those shown in Fig. 4b (for precipitation) and Fig. 6 (for circulation). These regression results further suggest that the precipitation and circulation changes between the two warming periods are closely linked to the meridional displacements of the two jets.

5. Mechanisms for the jet changes

The above analyses show that the jet displacements in recent decades may have affected the circulation and

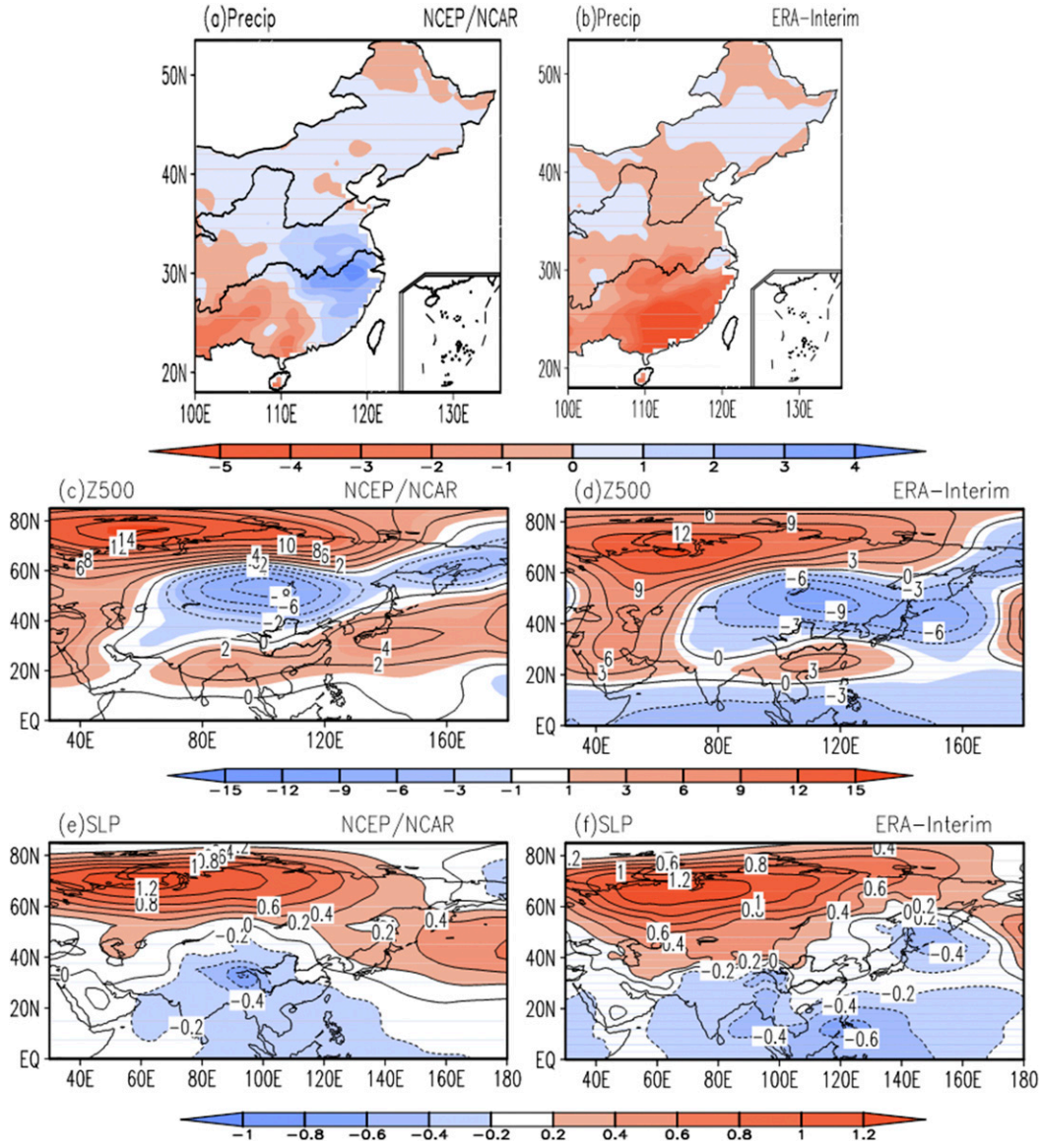

FIG. 10. The decadal changes in (a),(b) precipitation (mm); (c),(d) geopotential height at 500 hPa (gpm); and (e),(f) SLP (hPa) from 1985–98 to 1999–2013 estimated by multiplying the regression coefficients shown in Fig. 9 by the decadal changes in the position of the two jets shown Fig. 8 from the (left) NCEP–NCAR reanalysis and (right) ERA-Interim datasets.

precipitation in winter over eastern China. However, what causes the jet displacements is unclear. As discussed in the introduction, the MTG changes can play an important role in the variation of the two jets. Here we explored the linkage between the recent warming patterns and the displacements of the two jets.

Figure 11 shows the winter temperature change patterns from 1985–98 to 1999–2013. At the surface, a broad cooling is seen over the central and eastern Pacific and central Eurasia (Fig. 11a), similar to that seen in previous studies (e.g., Dai et al. 2015; C. Li et al. 2015). The temperature anomaly patterns over the Pacific Ocean resemble those associated with the negative phase of IPO (Power et al. 1999; Dai 2013; Dong and Dai 2015), as noticed previously by Dai et al. (2015). Substantial warming also exists over the Atlantic Ocean, and it resembles the positive phase of AMO (Dai et al. 2015). At upper levels (Figs. 11b,c), the temperature changes along the East Asian sector (70°–140°E) are characterized by the large warming over the high latitudes (north of 70°N, centered in the lower troposphere) and the low latitudes (south of ~40°N)

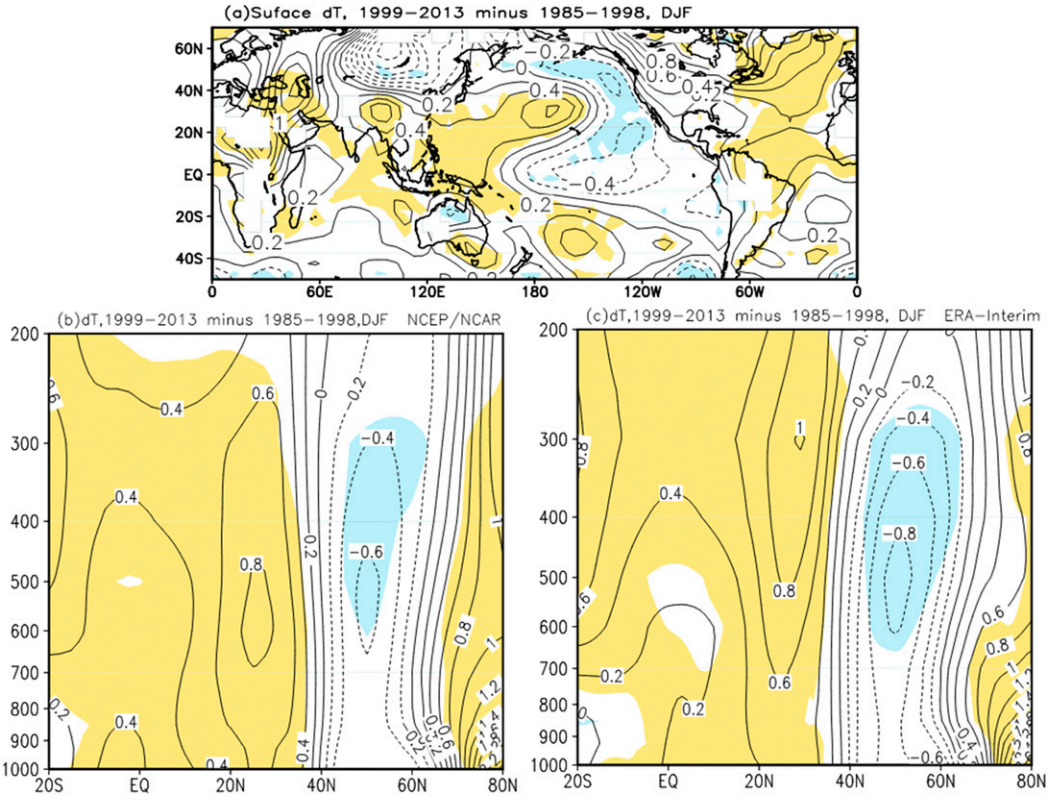

FIG. 11. The difference of DJF (a) surface temperature (°C) and the zonal mean air temperature averaged over East Asia (70°–140°E) between 1999–2013 and 1985–98 (°C) from the (b) NCEP–NCAR reanalysis and (c) ERA-Interim datasets. The shading indicates that the difference is significant at the 90% level.

and a cooling at the midlatitudes (45°–60°N). The large warming over the high latitudes is linked to the Arctic amplification of surface warming associated with sea ice loss (Serreze et al. 2009; Screen and Simmonds 2010), while the warming over the low latitudes is linked to the warming over the western Pacific and eastern Indian Ocean, where the warming is enhanced during an IPO cold phase (Dai 2013).

Since the surface temperature changes from 1985–98 to 1999–2013 resemble a combination of a negative IPO and a positive AMO (Fig. 11a), we first focused on the 300-hPa winds associated with the different groups of the IPO and AMO phase combination shown in Fig. 1. The composite 300-hPa wind speed anomalies in the four groups are shown in Fig. 12. In the "+IPO+AMO" group (Figs. 12a,b), positive wind anomalies at 300 hPa are in the active regions of the EAPJ, which enhance the EAPJ. In the "−IPO−AMO" group (Figs. 12e,f), no significant wind anomalies are seen over the active regions of the EAPJ and EASJ. Thus, neither of the two groups can be linked with the displacements of the EAPJ and EASJ. In contrast, in the "−IPO+AMO" (Figs. 12c,d) and "+IPO−AMO" (Figs. 12g,h) groups, a tripole anomaly pattern is along the active regions of the EASJ and EAPJ, with positive anomalies between them and negative anomalies to the south and north of it for the −IPO+AMO case. This pattern, in particular one shown in Figs. 12i,j for the −IPO+AMO minus +IPO−AMO case, assembles the 300-hPa wind differences between the two warming periods (Fig. 7). This result further links the recent wind changes to the negative IPO and positive AMO phase combination during the hiatus period.

Figure 13 shows the patterns of regressed 300-hPa wind speed against the normalized IPO or AMO index. Associated with the negative phase of IPO (Figs. 13a,b), there is an alternating anomaly pattern in 300-hPa wind speed with strengthened winds around 30°–47.5°N (midlatitude) and weakened winds to the north and south of it. This pattern is also evident for a positive phase of AMO (Figs. 13c,d). This alternating anomaly pattern should lead to an equatorward shift of the EAPJ and a poleward shift of the EASJ, as winds strengthen equatorward around the EAPJ box but poleward around the EASJ box. To further

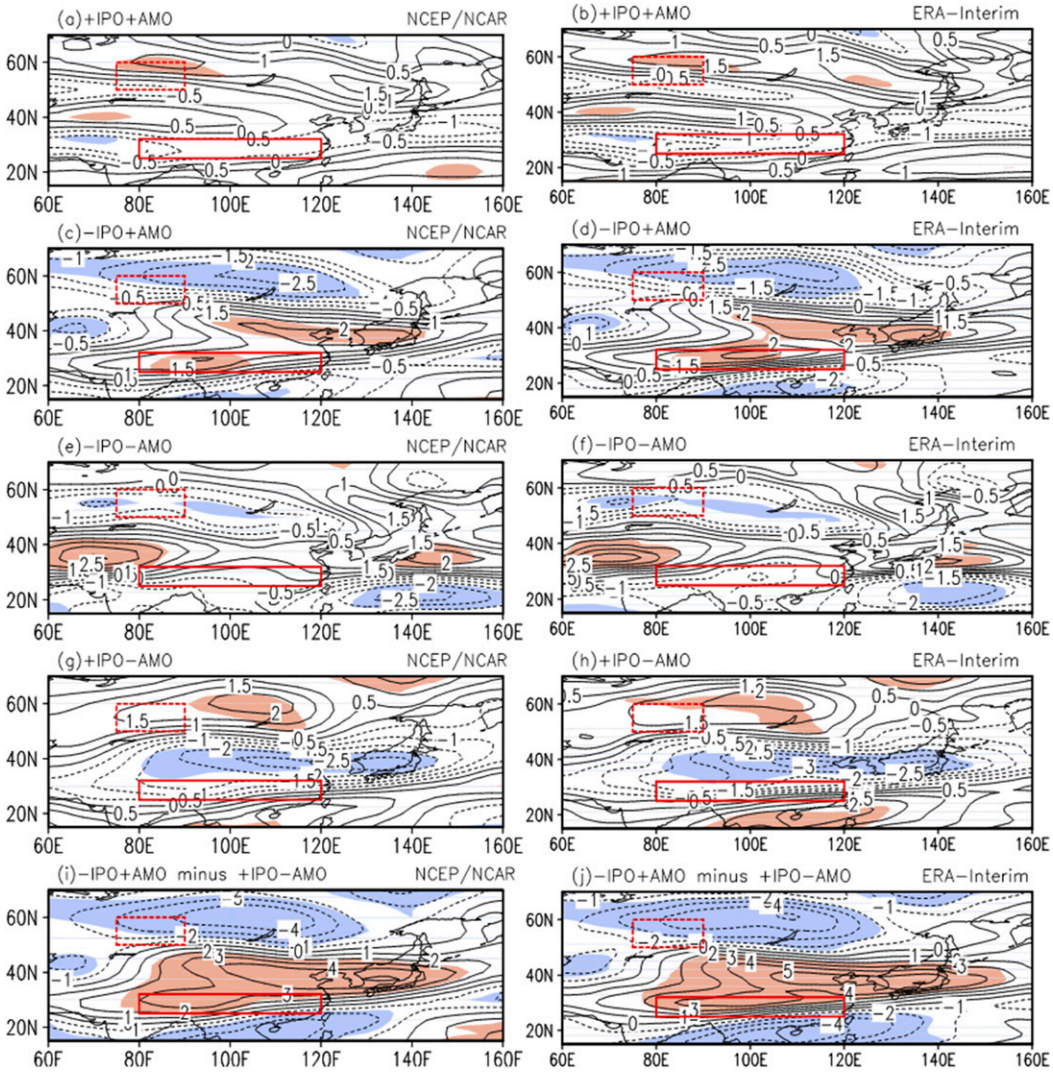

FIG. 12. Composite DJF wind speed anomalies (relative to 1985–2013 mean; m s^{-1}) at 300 hPa for the case of (a),(b) +IPO+AMO; (c),(d) −IPO+AMO; (e),(f) −IPO−AMO; and (g),(h) +IPO−AMO during the period of 1985–2013; and (i),(j) the composite DJF wind speed differences at 300 hPa between the −IPO+AMO and +IPO−AMO cases from the (left) NCEP–NCAR reanalysis and (right) ERA-Interim datasets. The shading indicates that the anomaly is significant at the 90% level. The red solid (dashed) box indicates the active regions of the EASJ (EAPJ).

quantify the contribution of the IPO and AMO to the decadal changes in 300-hPa winds, we multiplied the regression coefficients shown in Figs. 13a–d by the decadal changes of the IPO and AMO indices from 1985–98 to 1999–2013. Since the IPO and AMO indices are significantly correlated during 1985–2013 ($r = -0.48$), we showed the results separately for the IPO and AMO in Fig. 14 instead of combining them: that is, the contribution of the correlated part in the IPO and AMO indices is included in both cases for the IPO and AMO. The wind change patterns in Fig. 14 are broadly consistent with those in Fig. 7. This suggests that the wind changes and, in particular, the meridional displacements of the two jets are closely linked to the recent changes in the IPO and AMO.

Figure 15 shows the regression patterns of the mean MTG averaged from the surface to 300 hPa against the normalized IPO and AMO indices separately. The climatological MTG is negative over the Northern Hemisphere because of the decreasing temperature from south to north. Thus, associated with a negative IPO and a positive AMO index, the negative MTG anomaly over the midlatitude regions of 25°–50°N (Figs. 13a–d) would intensify the MTG and thus strengthen the westerlies

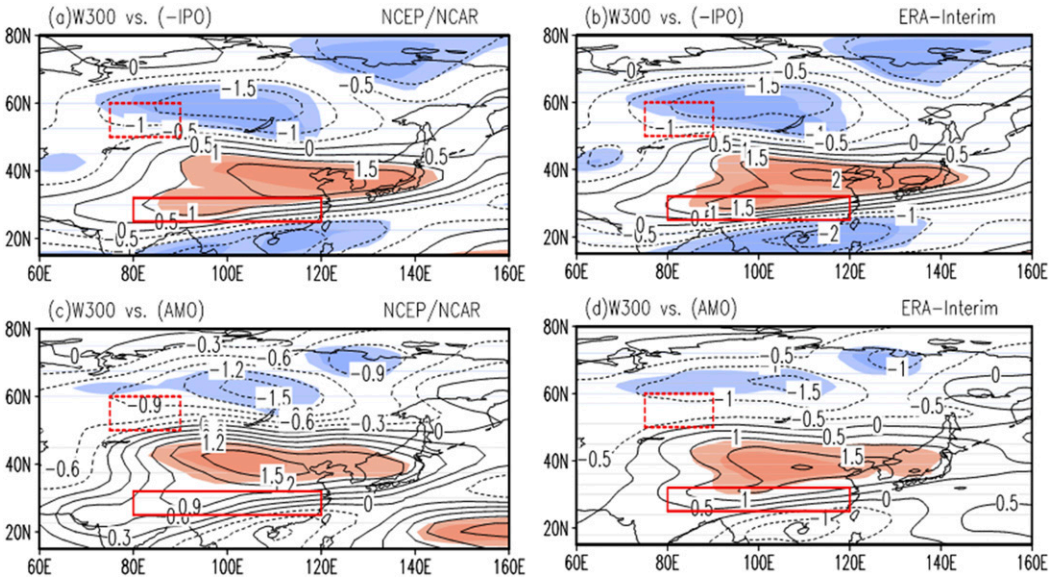

FIG. 13. Regression coefficients of DJF wind speed at 300 hPa (W300; m s^{-1} per unit index) against (a),(b) the normalized IPO index (multiplied by −1, indicating the negative phase of IPO) and (c),(d) normalized AMO index (m s^{-1}) during 1985–2013 from the (left) NCEP–NCAR reanalysis and (right) ERA-Interim. The red solid (dashed) box indicates the active regions of the EASJ (EAPJ). The shading in (a)–(d) indicates that the regression coefficient is significant at the 90% level.

there via the thermal wind relation. Meanwhile, the positive MTG anomalies over high and low latitudes would weaken the westerlies there. The effect of the IPO and AMO changes on the MTG is shown in Fig. 16, which is broadly consistent with the decadal MTG changes from 1985–98 to 1999–2013 estimated directly from the reanalysis data (Fig. 17). This indicates that the decadal MTG changes between the two periods are closely linked to the recent changes in the IPO and AMO and further suggests that the IPO and AMO changes are behind the decadal changes in the wind fields and the displacements of the two jets via their influences on the MTG.

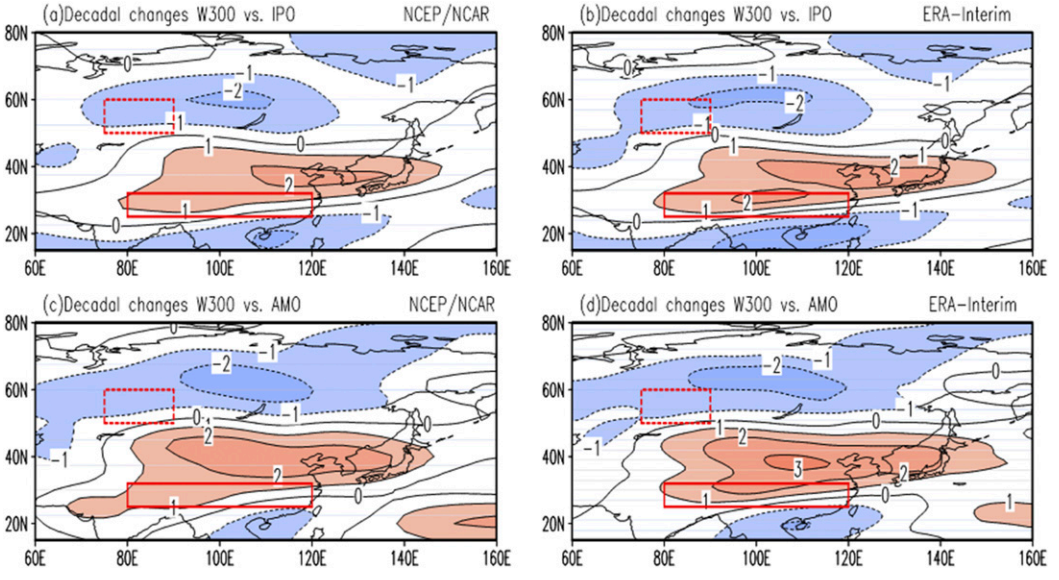

FIG. 14. The decadal changes of W300 (m s^{-1}) estimated by multiplying the regression coefficients shown in Figs. 13a–d by decadal changes in the (a),(b) IPO and (c),(d) AMO indices from 1985–98 to 1999–2013 from the (left) NCEP–NCAR reanalysis and (right) ERA-Interim. The red solid (dashed) box indicates the active regions of the EASJ (EAPJ).

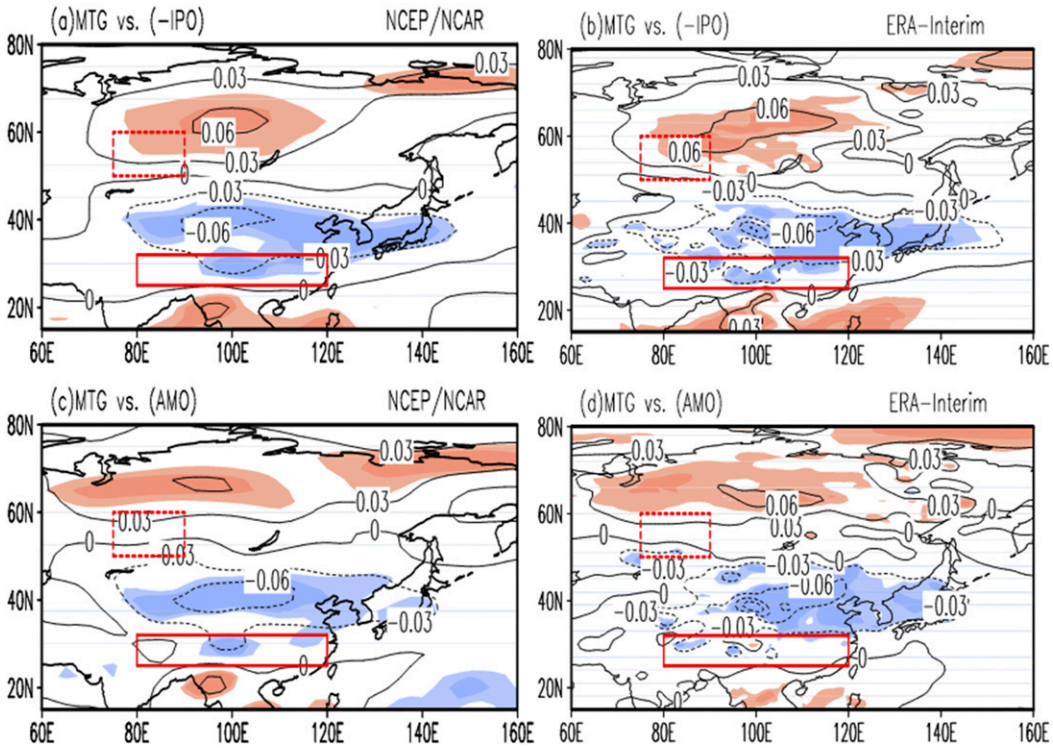

FIG. 15. As in Fig. 13, but for the regression patterns of DJF mean MTG averaged from the surface to 300 hPa (10^{-5} K m^{-1}).

A significant tripole anomaly pattern of 300-hPa wind speed (Figs. 18a,b) is associated with the vertical warming, which is defined in section 2. This pattern is comparable to that shown in Fig. 7, with some differences in the high latitudes (north of 50°N). In particular, the regressed wind pattern (Figs. 18a,b) shows large decreases over the active regions of the EAPJ. We also performed a regression of the MTG against the normalized vertical warming to investigate the possible mechanism for the meridional displacements of the two jets. As shown in Figs. 18c,d, the MTG changes associated with the changes in the vertical warming are broadly consistent with those shown in Fig. 17. This indicates that the changes of MTG are also closely linked to the changes of the vertical warming and thus lead to the meridional displacement of the two jets. The 300-hPa wind speed and MTG changes associated with the decadal changes of the vertical warming (not shown) are similar to the regressed pattern shown in Fig. 18.

6. Conclusions and discussion

Global-mean surface temperature has experienced a fast warming period of 1985–98 and a hiatus period of 1999–2013, especially for boreal winter. Compared with the fast warming period, winter precipitation has decreased by about 25% (increased by ~50%) over the southern (northeastern) part of eastern China during the hiatus period. This anomaly pattern reduces the south–north precipitation gradient seen in winter precipitation climatology. This recent regime shift of winter precipitation complements studies on decadal variations of the EAWM (e.g., Ding et al. 2014), since most previous studies used atmospheric circulation indices to quantify the EAWM changes.

We have examined the associated changes in atmospheric circulation, including the combined effect of the EASJ and EAPJ on winter precipitation over eastern China. From 1985–98 to 1999–2013, a negative–positive–negative pattern of change for wind speed at 300 hPa occurs from 20° to 60°N over East Asia, with strengthened winds around 30°–47.5°N and weakened winds to the north and south of it. This change pattern helps explain the equatorward (poleward) displacement of the EAPJ (EASJ) from the fast warming to the hiatus period. Associated with the wind changes and the meridional displacements of the two jets, the Siberian high enhances, and the East Asian trough shifts westward during the hiatus period. The enhanced Siberian high strengthens the East Asian winter monsoon (EAWM) and weakens southwesterly winds over the South China Sea, which decreases precipitation over

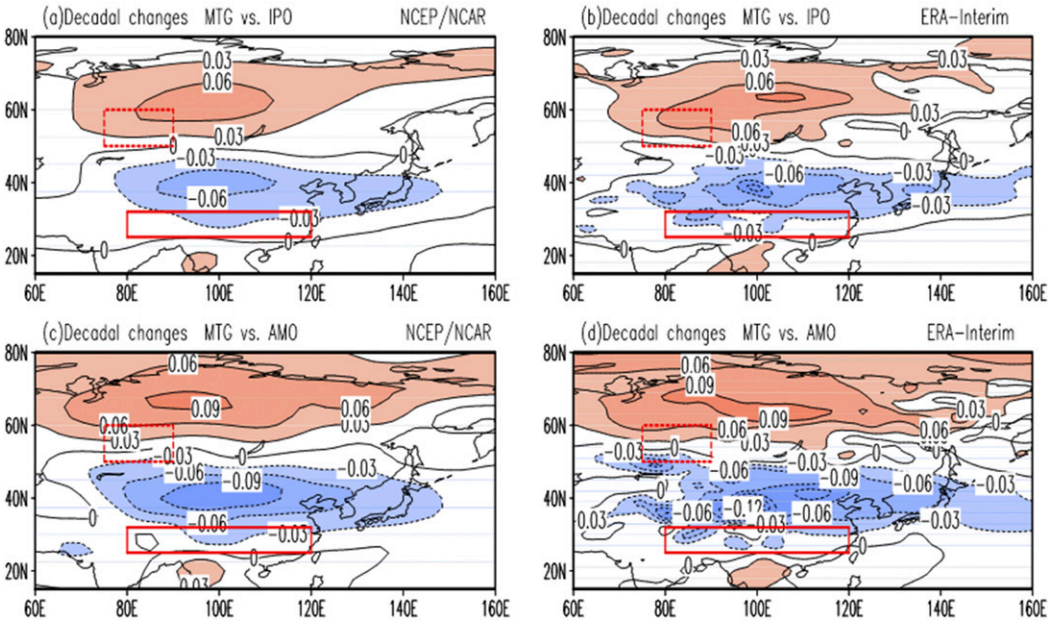

FIG. 16. As in Fig. 14, but for the estimated contribution to the MTG by the IPO and AMO via regression (10^{-5} K m^{-1}).

southern China. The westward shift of the East Asian trough enhances convergence over northeastern China, leading to increased precipitation there. These circulation changes provide favorable conditions for the northeastern-wet–southern-dry anomaly pattern during the hiatus period.

We have further examined the linkage between the wind changes (including the meridional displacements of the EAPJ and EASJ) and the changes in meridional temperature gradients (MTGs). For surface temperature changes between the two periods, the dominant feature is a combination of the temperature anomalies associated with a negative IPO phase and a positive AMO phase. In the free troposphere, a tripole temperature anomaly pattern exists over East Asia (70°–140°E), with warming over the low (south of ~40°N) and high (north of ~70°N) latitudes and cooling over the midlatitudes (45°–60°N). These temperature anomalies enhance the MTG and thus westerly winds over the region between the two jets but weaken the MTG and thus the westerlies to the south and north of it. These MTG-induced changes help explain the abovementioned wind anomaly patterns and the displacements of the two jets.

The decadal changes in temperature and wind fields have been further linked to recent phase changes of the IPO and AMO. Specifically, a negative IPO phase and a positive AMO phase during the hiatus period led to the warming at the low and high latitudes and cooling at the midlatitudes over the East Asian sector. Thus, we concluded that the IPO and AMO can significantly influence winter tropospheric MTG and thus circulation fields (including EAWM and the EAPJ and EASJ) over East Asia, which in turn affect winter

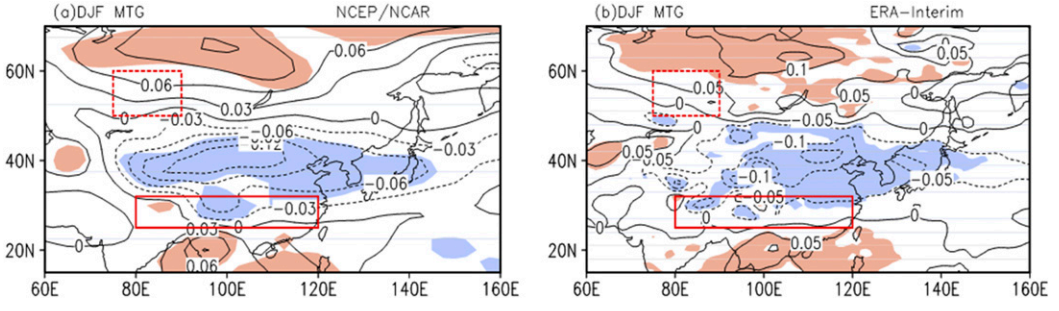

FIG. 17. The difference of DJF mean MTG (10^{-5} K m^{-1}) averaged from the surface to 300 hPa between 1999–2013 and 1985–98 from (a) NCEP–NCAR reanalysis and (b) ERA-Interim. The red solid (dashed) box indicates the active regions of the EASJ (EAPJ). The shading indicates that the difference is significant at the 90% level.

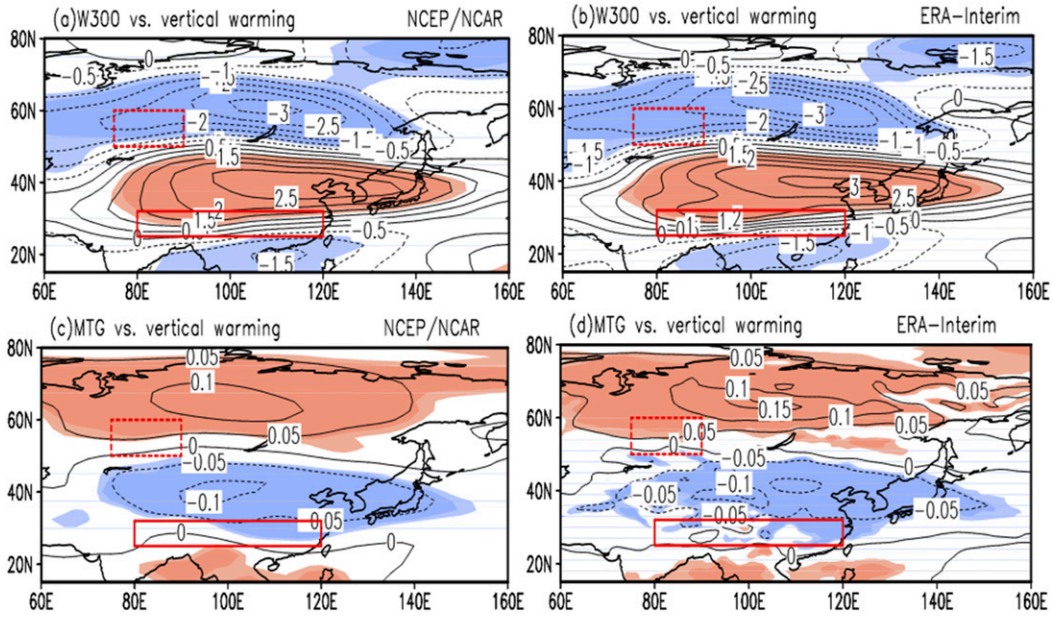

FIG. 18. Regression coefficients of (a),(b) DJF W300 ($m\,s^{-1}$ per unit warming) and (c),(d) MTG averaged from surface to 300 hPa ($10^{-5}\,K\,m^{-1}$) against the normalized vertical warming in 1985–2013 from (left) NCEP–NCAR reanalysis and (right) ERA-Interim. The red solid (dashed) box indicates the active regions of the EASJ (EAPJ). The shading indicates that the regression coefficient is significant at the 90% level.

precipitation over eastern China, and that the recent northeastern-wet–southern-dry anomaly pattern since 1999 results largely from the combined effect of a negative IPO phase and a positive AMO phase during this period.

It should be emphasized that the observational and reanalysis data used here include impacts from the Indian Ocean, the tropical SSTs of which are rising due to global warming and also vary with the IPO (Dong et al. 2016), and they are related to the recent wet anomaly over the Yangtze River delta (X.-F. Li et al. 2015). Thus, the relationship between the IPO or AMO and the variations of the two jets revealed here include the role of the Indian Ocean. Numerical experiments are underway to quantify the relative contributions of the warming trend in the Indian Ocean and the decadal SST variations associated with the IPO in the Pacific and Indian Ocean and the AMO in the North Atlantic Ocean.

Acknowledgments. This study is jointly sponsored by the National Key Research and Development Program of China (Grant 2016YFA0600701), the National Natural Science Foundation of China (Grants 41130963 and 41575071), and the Jiangsu Collaborative Innovation Center for Climate Change. A. Dai is supported by the U.S. National Science Foundation (Grant AGS-1353740), U.S. Department of Energy's Office of Science (Award DE-SC0012602), and the U.S. National Oceanic and Atmospheric Administration (Award NA15OAR4310086). We are grateful to the three anonymous reviewers for their helpful suggestions on improving our work.

REFERENCES

Ao, J., and J. Sun, 2016: Decadal change in factors affecting winter precipitation over eastern China. *Climate Dyn.*, **46**, 111–121, doi:10.1007/s00382-015-2572-7.

Chan, J. C. L., and C. Y. Li, 2004: The East Asia winter monsoon. *East Asian Monsoon*, C. P. Chang, Ed., World Scientific Series on Asia-Pacific Weather and Climate, Vol. 2, World Scientific Publishing Co., 54–106.

Chen, W., J. Feng, and R. Wu, 2013: Roles of ENSO and PDO in the link of the East Asian winter monsoon to the following summer monsoon. *J. Climate*, **26**, 622–635, doi:10.1175/JCLI-D-12-00021.1.

Dai, A., 2013: The influence of the inter-decadal Pacific oscillation on US precipitation during 1923–2010. *Climate Dyn.*, **41**, 633–646, doi:10.1007/s00382-012-1446-5.

——, J. C. Fyfe, S.-P. Xie, and X. Dai, 2015: Decadal modulation of global surface temperature by internal climate variability. *Nat. Climate Change*, **5**, 555–559, doi:0.1038/nclimate2605.

Dee, D. P., and Coauthors, 2011: The ERA-Interim reanalysis: Configuration and performance of the data assimilation system. *Quart. J. Roy. Meteor. Soc.*, **137**, 553–597, doi:10.1002/qj.828.

Ding, Y., and J. C. L. Chan, 2005: The East Asian summer monsoon: An overview. *Meteor. Atmos. Phys.*, **89**, 117–142, doi:10.1007/s00703-005-0125-z.

——, Z. Wang, and Y. Sun, 2008: Inter-decadal variation of the summer precipitation in East China and its association with decreasing Asian summer monsoon. Part I: Observed evidences. *Int. J. Climatol.*, **28**, 1139–1161, doi:10.1002/joc.1615.

——, Y. Sun, Z. Wang, and Y. Song, 2009: Inter-decadal variation of the summer precipitation in China and its association with decreasing Asian summer monsoon. Part II: Possible causes. *Int. J. Climatol.*, **29**, 1926–1944, doi:10.1002/joc.1759.

——, and Coauthors, 2014: Interdecadal variability of the East Asian winter monsoon and its possible links to global climate change. *J. Meteor. Res.*, **28**, 693–713, doi:10.1007/s13351-014-4046-y.

Dong, B., and A. Dai, 2015: The influence of the interdecadal Pacific oscillation on temperature and precipitation over the globe. *Climate Dyn.*, **45**, 2667–2681, doi:10.1007/s00382-015-2500-x.

Dong, L., T. Zhou, A. Dai, F. Song, B. Wu, and X. Chen, 2016: The footprint of the inter-decadal Pacific oscillation in Indian Ocean sea surface temperatures. *Sci. Rep.*, **6**, 21251, doi:10.1038/srep21251.

Du, Y., Y. Zhang, and Z. Xie, 2009: Impacts of the zonal position of the East Asian westerly jet core on precipitation distribution during Meiyu of China. *Acta Meteor. Sin.*, **23**, 506–516.

England, M. H., and Coauthors, 2014: Recent intensification of wind-driven circulation in the Pacific and the ongoing warming hiatus. *Nat. Climate Change*, **4**, 222–227, doi:10.1038/nclimate2106.

Feng, L., T. Li, and W. Yu, 2014: Cause of severe droughts in Southwest China during 1951–2010. *Climate Dyn.*, **43**, 2033–2042, doi:10.1007/s00382-013-2026-z.

Fyfe, J. C., N. P. Gillett, and G. J. Marshall, 2012: Human influence on extratropical Southern Hemisphere summer precipitation. *Geophys. Res. Lett.*, **39**, L23711, doi:10.1029/2012GL054199.

Ge, J., X. Jia, and H. Lin, 2016: The interdecadal change of the leading mode of the winter precipitation over China. *Climate Dyn.*, **47**, 2397–2411, doi:10.1007/s00382-015-2970-x.

Gillett, N. P., V. K. Arora, G. M. Flato, J. F. Scinocca, and K. von Salzen, 2012: Improved constraints on 21st-century warming derived using 160 years of temperature observations. *Geophys. Res. Lett.*, **39**, L01704, doi:10.1029/2011GL050226.

Ha, K.-J., K.-Y. Heo, S.-S. Lee, K.-S. Yun, and J.-G. Jhun, 2012: Variability in the East Asian monsoon: A review. *Meteor. Appl.*, **19**, 200–215, doi:10.1002/met.1320.

Hartmann, D. L., and Coauthors, 2013: Observations: Atmosphere and surface. *Climate Change 2013: The Physical Science Basis*, T. F. Stocker et al., Eds., Cambridge University Press, 159–254. [Available online at http://www.climatechange2013.org/images/report/WG1AR5_Chapter02_FINAL.pdf.]

Holton, J. R., J. Pyle, and J. A. Curry, 2002: *Encyclopedia of Atmospheric Sciences*. Academic Press, 1043–1055.

Huang, D.-Q., J. Zhu, Y.-C. Zhang, and A. Huang, 2014: The different configurations of the East Asian polar front jet and subtropical jet and the associated rainfall anomalies over Eastern China in summer. *J. Climate*, **27**, 8205–8220, doi:10.1175/JCLI-D-14-00067.1.

——, ——, ——, J. Wang, and X.-Y. Kuang, 2015: The impact of the East Asian subtropical jet and polar front jet on the frequency of spring persistent rainfall over southern China in 1997–2011. *J. Climate*, **28**, 6054–6066, doi:10.1175/JCLI-D-14-00641.1.

Huang, R., L. Zhou, and W. Chen, 2003: The progresses of recent studies on the variabilities of the East Asian monsoon and their causes. *Adv. Atmos. Sci.*, **20**, 55–69, doi:10.1007/BF03342050.

——, Y. Liu, H. Jingliang, and T. Feng, 2014: Characteristics and internal dynamical causes of the interdecadal variability of East Asian winter monsoon near the late 1990s (in Chinese). *Chin. J. Atmos. Sci.*, **38**, 627–644.

Hudson, R. D., 2012: Measurements of the movement of the jet streams at mid-latitudes, in the Northern and Southern Hemispheres, 1979 to 2010. *Atmos. Chem. Phys.*, **12**, 7797–7808, doi:10.5194/acp-12-7797-2012.

Kalnay, E., and Coauthors, 1996: The NCEP/NCAR 40-Year Reanalysis Project. *Bull. Amer. Meteor. Soc.*, **77**, 437–471, doi:10.1175/1520-0477(1996)077<0437:TNYRP>2.0.CO;2.

Karl, T. R., and Coauthors, 2015: Possible artifacts of data biases in the recent global surface warming hiatus. *Science*, **348**, 1469–1472, doi:10.1126/science.aaa5632.

Kendall, M., 1975: *Rank Correlation Methods*. 4th ed. Charles Griffin, 210 pp.

Kim, J.-W., S.-W. Yeh, and E.-C. Chang, 2014: Combined effect of El Niño–Southern Oscillation and Pacific decadal oscillation on the East Asian winter monsoon. *Climate Dyn.*, **42**, 957–971, doi:10.1007/s00382-013-1730-z.

Kosaka, Y., and S.-P. Xie, 2013: Recent global-warming hiatus tied to equatorial Pacific surface cooling. *Nature*, **501**, 403–407, doi:10.1038/nature12534.

Kuang, X., and Y. Zhang, 2006: Impact of the position abnormalities of East Asian subtropical westerly jet on summer precipitation in middle-lower reaches of Yangtze River (in Chinese). *Plateau Meteor.*, **25**, 382–389.

——, ——, and J. Liu, 2008: Relationship between subtropical upper-tropospheric westerly jet and East Asian winter monsoon (in Chinese). *Plateau Meteor.*, **27**, 701–712.

Li, C., B. Stevens, and J. Marotzke, 2015: Eurasian winter cooling in the warming hiatus of 1998–2012. *Geophys. Res. Lett.*, **42**, 8131–8139, doi:10.1002/2015GL065327.

Li, L., and Y. Zhang, 2014: Effects of different configurations of the East Asian subtropical and polar front jets on precipitation during Meiyu season. *J. Climate*, **27**, 6660–6672, doi:10.1175/JCLI-D-14-00021.1.

——, B. Wang, and T. Zhou, 2007: Impacts of external forcing on the 20th century global warming. *Chin. Sci. Bull.*, **52**, 3148–3154, doi:10.1007/s11434-007-0463-y.

Li, S., and G. T. Bates, 2007: Influence of the Atlantic multidecadal oscillation on the winter climate of East China. *Adv. Atmos. Sci.*, **24**, 126–135, doi:10.1007/s00376-007-0126-6.

Li, X.-F., J. Li, and Y. Li, 2015: Recent winter precipitation increase in middle–lower Yangtze River valley since the late 1970s: A response to warming in tropical Indian Ocean. *J. Climate*, **28**, 3857–3879, doi:10.1175/JCLI-D-14-00701.1.

Liang, S., Y. Ding, N. Zhao, and Y. Sun, 2014: Analysis of the interdecadal changes of the wintertime surface air temperature over mainland China and regional atmospheric circulation characteristics during 1960–2013 (in Chinese). *Chin. J. Atmos. Sci.*, **38**, 974–992.

Liao, Z., and Y. Zhang, 2013: Concurrent variation between the East Asian subtropical jet and polar front jet during persistent snowstorm period in 2008 winter over southern China. *J. Geophys. Res.*, **118**, 6360–6373, doi:10.1002/jgrd.50558.

Liu, Z., 2012: Dynamics of interdecadal climate variability: A historical perspective. *J. Climate*, **25**, 1963–1995, doi:10.1175/2011JCLI3980.1.

Lu, R., Z. Lin, and Y. Zhang, 2013: Variability of the East Asian upper-tropospheric jet in summer and its impacts on the East Asian monsoon (in Chinese). *Chin. J. Atmos. Sci.*, **37**, 331–340.

Luo, X., and Y. Zhang, 2015: The linkage between upper-level jet streams over East Asia and East Asian winter monsoon variability. *J. Climate*, **28**, 9013–9028, doi:10.1175/JCLI-D-15-0160.1.

Ma, T., Z. Wu, and Z. Jiang, 2012: How does coldwave frequency in China respond to a warming climate? *Climate Dyn.*, **39**, 2487–2496, doi:10.1007/s00382-012-1354-8.

Mann, H., 1945: Nonparametric tests against trend. *Econometrica*, **13**, 245–259, doi:10.2307/1907187.

Mao, R., D. Gong, and Q. Fang, 2007: Influences of the East Asian jet stream on winter climate in China (in Chinese). *J. Appl. Meteor. Sci.*, **18**, 137–146.

Meehl, G. A., A. Hu, B. D. Santer, and S.-P. Xie, 2016: Contribution of the interdecadal Pacific oscillation to twentieth-century global surface temperature trends. *Nat. Climate Change*, **6**, 1005–1008, doi:10.1038/nclimate3107.

Morice, C. P., J. J. Kennedy, N. A. Rayner, and P. D. Jones, 2012: Quantifying uncertainties in global and regional temperature change using an ensemble of observational estimates: The HadCRUT4 data set. *J. Geophys. Res.*, **117**, D08101, doi:10.1029/2011JD017187.

North, G. R., T. L. Bell, and R. F. Cahalan, 1982: Sampling errors in the estimation of empirical orthogonal functions. *Mon. Wea. Rev.*, **110**, 669–706, doi:10.1175/1520-0493(1982)110<0699:SEITEO>2.0.CO;2.

Overland, J. E., and M. Wang, 2010: Large-scale atmospheric circulation changes are associated with the recent loss of Arctic sea ice. *Tellus*, **62A**, 1–9, doi:10.1111/j.1600-0870.2009.00421.x.

Power, S., T. Casey, C. Folland, A. Colman, and V. Mehta, 1999: Inter-decadal modulation of the impact of ENSO on Australia. *Climate Dyn.*, **15**, 319–324, doi:10.1007/s003820050284.

Rayner, N. A., D. E. Parker, E. B. Horton, C. K. Folland, L. V. Alexander, D. P. Rowell, E. C. Kent, and A. Kaplan, 2003: Global analyses of sea surface temperature, sea ice, and night marine air temperature since the late nineteenth century. *J. Geophys. Res.*, **108**, 4407, doi:10.1029/2002JD002670.

Ren, X., X. Yang, and C. Chu, 2010: Seasonal variations of the synoptic-scale transient eddy activity and polar front jet over East Asia. *J. Climate*, **23**, 3222–3233, doi:10.1175/2009JCLI3225.1.

——, ——, T. Zhou, and J. Fang, 2011: Diagnostic comparison of wintertime East Asian subtropical jet and polar-front jet: Large-scale characteristics and transient eddy activities. *Acta Meteor. Sin.*, **25**, 21–33, doi:10.1007/s13351-011-0002-2.

Santer, B. D., and Coauthors, 2011: Separating signal and noise in atmospheric temperature changes: The importance of timescale. *J. Geophys. Res.*, **116**, D22105, doi:10.1029/2011JD016263.

Screen, J. A., and I. Simmonds, 2010: The central role of diminishing sea ice in recent Arctic temperature amplification. *Nature*, **464**, 1334–1337, doi:10.1038/nature09051.

Seidel, D., Q. Fu, W. Randel, and T. Reichler, 2008: Widening of the tropical belt in a changing climate. *Nat. Geosci.*, **1**, 21–24, doi:10.1038/ngeo.2007.38.

Serreze, M. C., A. P. Barrett, J. C. Stroeve, D. N. Kindig, and M. M. Holland, 2009: The emergence of surface-based Arctic amplification. *Cryosphere*, **3**, 11–19, doi:10.5194/tc-3-11-2009.

Shao, P., and D. Li, 2012: Classification and comparison of East Asian winter monsoon indices (in Chinese). *J. Meteor. Sci.*, **32**, 226–235.

Si, D., Y. Ding, and Y. Liu, 2009: Decadal northward shift of the Meiyu belt and the possible cause. *Chin. Sci. Bull.*, **54**, 4742–4748, doi:10.1007/s11434-009-0385-y.

Solomon, S., J. S. Daniel, R. R. Neely, J.-P. Vernier, E. G. Dutton, and L. W. Thomason, 2011: The persistently variable "background" stratospheric aerosol layer and global climate change. *Science*, **333**, 866–870, doi:10.1126/science.1206027.

Steinman, B. A., M. E. Mann, and S. K. Miller, 2015: Atlantic and Pacific multidecadal oscillations and Northern Hemisphere temperatures. *Science*, **347**, 988–991, doi:10.1126/science.1257856.

Sun, J., and J. Ao, 2013: Changes in precipitation and extreme precipitation in a warming environment in China. *Chin. Sci. Bull.*, **58**, 1395–1401, doi:10.1007/s11434-012-5542-z.

——, H. Wang, W. Yuan, and H. Chen, 2010: Spatial-temporal features of intense snowfall events in China and their possible change. *J. Geophys. Res.*, **115**, D16110, doi:10.1029/2009JD013541.

——, S. Wu, and J. Ao, 2015: Role of the North Pacific sea surface temperature in the East Asian winter monsoon decadal variability. *Climate Dyn.*, **46**, 3799–3805, doi:10.1007/s00382-015-2805-9.

Tao, S., and Q. Zhang, 1998: Response of the Asian winter and summer monsoon to ENSO events (in Chinese). *Sci. Atmos. Sin.*, **22**, 399–407.

Trenberth, K. E., and J. T. Fasullo, 2013: An apparent hiatus in global warming? *Earth's Future*, **1**, 19–32, doi:10.1002/2013EF000165.

Wallace, J. M., and P. V. Hobbs, 2005: *Atmospheric Science: An Introductory Survey*. 2nd ed. Elsevier, 483 pp.

Wang, B., Z. Zhu, C. Chin-Pei, J. Liu, J. Li, and T. Zhou, 2010: Another look at interannual-to-interdecadal variations of the East Asian winter monsoon: The northern and southern temperature modes. *J. Climate*, **23**, 1495–1512, doi:10.1175/2009JCLI3243.1.

Wang, H., and K. Fan, 2013: Recent Changes in the East Asian Monsoon (in Chinese). *Chin. J. Atmos. Sci.*, **37**, 313–318.

——, and S. He, 2013: The increase of snowfall in northeast China after the mid-1980s. *Chin. Sci. Bull.*, **58**, 1350–1354, doi:10.1007/s11434-012-5508-1.

Wang, L., and W. Chen, 2010: How well do existing indices measure the strength of the East Asian winter monsoon? *Adv. Atmos. Sci.*, **27**, 855–870, doi:10.1007/s00376-009-9094-3.

——, and J. Feng, 2011: Two major modes of the wintertime precipitation over China (in Chinese). *Chin. J. Atmos. Sci.*, **35**, 1105–1116.

——, W. Chen, and R. Huang, 2008: Interdecadal modulation of PDO on the impact of ENSO on the East Asian winter monsoon. *Geophys. Res. Lett.*, **35**, L20702, doi:10.1029/2008GL035287.

Wang, N., and Y. Zhang, 2015: Connections between the Eurasian teleconnection and concurrent variation of upper-level jets over East Asia. *Adv. Atmos. Sci.*, **32**, 336–348, doi:10.1007/s00376-014-4088-1.

Watanabe, M., Y. Kamae, and M. Kimoto, 2014: Robust increase of the equatorial Pacific rainfall and its variability in a warmed climate. *Geophys. Res. Lett.*, **41**, 3227–3232, doi:10.1002/2014GL059692.

Woollings, T., 2008: Vertical structure of anthropogenic zonal-mean atmospheric circulation change. *Geophys. Res. Lett.*, **35**, L19702, doi:10.1029/2008GL034883.

——, B. Harvey, and G. Masato, 2014: Arctic warming, atmospheric blocking and cold European winters in CMIP5 models. *Environ. Res. Lett.*, **9**, 014002, doi:10.1088/1748-9326/9/1/014002.

Xiao, C., and Y. Zhang, 2015: Projected changes of wintertime synoptic-scale transient eddy activities in the East Asian

eddy-driven jet from CMIP5 experiments. *Geophys. Res. Lett.*, **42**, 6008–6013, doi:10.1002/2015GL064641.

Xin, X., R. Yu, T. Zhou, and W. Bin, 2006: Drought in late spring of South China in recent decades. *J. Climate*, **19**, 3197–3206, doi:10.1175/JCLI3794.1.

Yao, H., and D. Li, 2013: The relationship between Asian jets and the winter monsoon and their impact on climate in China (in Chinese). *Acta Meteor. Sin.*, **71**, 429–439.

Yim, B. Y., H. S. Min, and J.-S. Kug, 2015: Inter-model diversity in jet stream changes and its relation to Arctic climate in CMIP5. *Climate Dyn.*, **47**, 235–248, doi:10.1007/s00382-015-2833-5.

Yu, R., and T. Zhou, 2007: Seasonality and three-dimensional structure of interdecadal change in the East Asian monsoon. *J. Climate*, **20**, 5344–5355, doi:10.1175/2007JCLI1559.1.

Zeng, J., Q. Zhang, and T. Wang, 2010: Analysis on relationship of East-Asian Winter Monsoon intensity and winter precipitation in Southern China (in Chinese). *Plateau Meteor.*, **29**, 975–981.

Zhang, L., 2016: The roles of external forcing and natural variability in global warming hiatuses. *Climate Dyn.*, **47**, 3157–3169, doi:10.1007/s00382-016-3018-6.

Zhang, Y., and D. Huang, 2011: Has the East Asian westerly jet experienced a poleward displacement in recent decades? *Adv. Atmos. Sci.*, **28**, 1259–1265, doi:10.1007/s00376-011-9185-9.

——, K. R. Sperber, and J. S. Boyle, 1997: Climatology and interannual variation of the East Asian winter monsoon: Results from the 1979–95 NCEP/NCAR reanalysis. *Mon. Wea. Rev.*, **125**, 2605–2619, doi:10.1175/1520-0493(1997)125<2605:CAIVOT>2.0.CO;2.

——, D. Wang, and X. Ren, 2008: Seasonal variation of the meridional wind in the temperate jet stream and its relationship to the Asian monsoon. *Acta Meteor. Sin.*, **22**, 446–454.

Zhao, Y., J. Zhu, and Y. Xu, 2014: Establishment and assessment of the grid precipitation datasets in China for recent 50 years (in Chinese). *J. Meteor. Sci.*, **34**, 4–10.

Zhou, L.-T., 2011: Impact of East Asian winter monsoon on rainfall over southeastern China and its dynamical process. *Int. J. Climatol.*, **31**, 677–686, doi:10.1002/joc.2101.

——, and R. Wu, 2010: Respective impacts of the East Asian winter monsoon and ENSO on winter rainfall in China. *J. Geophys. Res.*, **115**, D02107, doi:10.1029/2009JD012502.

Zhou, T., D. Gong, J. Li, and B. Li, 2009: Detecting and understanding the multi-decadal variability of the East Asian summer monsoon—Recent progress and state of affairs. *Meteor. Z.*, **18**, 455–467, doi:10.1127/0941-2948/2009/0396.

Zhu, J., D. Huang, Yi. Dai, and X. Chen, 2015: Recent heterogeneous warming and the associated summer precipitation over eastern China. *Theor. Appl. Climatol.*, **123**, 619–627, doi:10.1007/s00704-015-1380-7.

Zou, J. S., J. Jing, and M. H. Wang, 1990: *Climatology in the Upper Atmosphere* (in Chinese). China Meteorological Press, 212 pp.